LRP 422/90 December 1990

ION CYCLOTRON MODES IN A LOW DENSITY PLASMA CAVITY. PART I : THEORY

M.L. Sawley

C R P P

ÉCOLE POLYTECHNIQUE FÉDÉRALE DE LAUSANNE - SUISSE

Ion cyclotron modes in a low density plasma cavity.
Part I : Theory

M.L. Sawley *

Centre de Recherches en Physique des Plasmas
Association Euratom-Confédération Suisse
Ecole Polytechnique Fédérale de Lausanne
21, Avenue des Bains, 1007 Lausanne, Switzerland

Abstract. Ion cyclotron modes excited in a low density, cylindrical plasma cavity using an external inductive antenna are investigated theoretically. These modes, which have a long parallel wavelength, exhibit a strong electrostatic character and are only weakly coupled to the antenna fields. It is shown that, despite the low frequency considered, electron dynamics play a dominant role via the effects of both Landau damping and electron inertia. The characteristics of the wavefields associated with these modes, relevant to an experimental investigation, are described.

* Present address: IMHEF-EPFL, ME-Ecublens, 1015 Lausanne, Switzerland

1. Introduction

The theoretical investigation of ion cyclotron wave propagation in a magnetized plasma has received extensive attention. Early work [1] was motivated by experiments that studied the absorption of ion cyclotron waves when propagated into a magnetic beach region (see the companion paper [2] for references to experimental investigations). The theory that neglected electron inertia (that is, assumed $m_e = 0$) was found to provide good agreement with experimental results for the high range of plasma density ($n_e \geq 2 \times 10^{12}$ cm^{-3}). However, for lower densities, electron inertia was shown [3], [4] to have a dominant influence on the ion cyclotron wave propagation. The observed heating of the ions in this early series of experiments was attributed to resonant ion cyclotron damping, and that of the electrons to both electron Landau damping and ion-electron collisions [5]. However, no attempt was made to develop a theory that included all of these dissipation effects. Thus, direct quantitative comparison of the measured ion cyclotron wavefields with theoretical predictions was not possible.

Many other theoretical investigations of the coupling of an inductive antenna to a magnetized plasma column have also been reported. Some studies [6] - [8] treated plasmas with more than one ion species, however, only collisional damping of the plasma was considered.

In the present paper, a theoretical investigation of the excitation of ion cyclotron waves, using an inductive antenna, in a magnetized plasma of low density ($n_e \leq 10^{12}$ cm^{-3}) is presented. In particular, a plasma containing more than one ion species is considered, with the excitation frequency in the vicinity of the corresponding ion cyclotron frequencies. For the conditions considered, the parallel wavelength of the ion cyclotron waves is very long (of the order of metres), except in the close vicinity of the cyclotron

frequencies. Since the wavelength is comparable to the length of the plasma column considered, axial standing waves are formed. Thus the present study treats cavity modes in the near field of the antenna, as opposed to the propagating waves investigated in the above-mentioned experiments. Even though these modes are essentially electrostatic in nature (k approximately parallel to E), due to the small electromagnetic component present they are weakly coupled to the antenna fields.

In Section 2, the theory for the electromagnetic excitation of ion cyclotron modes in a cylindrical cavity partially filled with a uniform plasma is outlined. Included in the theory are the effects of not only electron inertia, but also electron Landau damping and bulk electron drift. The ions are assumed to be cold, and suffer only collisional damping. With the experimental observation of these modes - described in the companion paper [2] - in mind, the results of calculations for a two ion species neon plasma are presented in Section 3.

2. Theory

We shall consider ion cyclotron modes in a cylindrical plasma cavity of length L and radius p imbedded in a uniform axial magnetic field B_0. The plasma is surrounded by a vacuum region and by a perfectly conducting cylindrical shell of radius q. The cavity is bounded in the axial direction by conducting end walls. The modes are excited by an antenna consisting of an azimuthal current sheet of radius s located in the vacuum region. A cylindrical, axially-conducting Faraday shield of radius u is located between the antenna and the plasma. A schematic diagram of the partially plasma filled cavity is shown in figure 1.

We shall consider axisymmetric (m=0) modes having a temporal dependence $\exp(i\omega t)$. After Fourier analysis in time, Maxwell's equations combine to give for the electric wavefield

$$\nabla \times \left(\nabla \times \mathbf{E} \right) = \frac{\omega^2}{c^2} \mathbf{K} \cdot \mathbf{E} \quad , \tag{1}$$

where **K** is the dielectric tensor.

Since the plasma is confined to the region $-L/2 \le z \le L/2$, solutions of equation (1) for the electric field components may be expressed in terms of finite Fourier series. We write

$$\begin{aligned} E_{r,\theta} &= \sum_{n=1}^{\infty} e_{r,\theta}^{n} \sin \frac{n\pi}{L} z \quad , \\ E_z &= \frac{1}{2} e_z^0 + \sum_{n=1}^{\infty} e_z^n \cos \frac{n\pi}{L} z \quad . \end{aligned} \tag{2}$$

These forms have been chosen to satisfy the boundary conditions at the end conducting walls, namely,

$$E_r(z = \pm L/2) = E_\theta(z = \pm L/2) = 0 \quad . \tag{3}$$

Similarly, we write for the magnetic wavefield components

$$\begin{aligned} B_{r,\theta} &= \frac{1}{2} b_{r,\theta}^0 + \sum_{n=1}^{\infty} b_{r,\theta}^n \cos \frac{n\pi}{L} z \quad , \\ B_z &= \sum_{n=1}^{\infty} b_z^n \sin \frac{n\pi}{L} z \quad . \end{aligned} \tag{4}$$

We now proceed by solving equation (1) in each of the regions shown in figure 1.

(i) In the plasma region I :

We shall consider a uniform plasma comprised of more than one ion species. Each of the ion species is considered to be cold ($T_i = 0$), and thus we neglect the effect of ion cyclotron damping. However, collisional damping of each ion species with the stationary background (corresponding, for example, to collisions with neutral atoms) is accounted for by introducing an effective collision frequency ν_i. It is assumed that the collision frequency is the same for all the ion species.

The electron species is assumed to to be warm, with an isotropic temperature distribution ($T_{e\perp} = T_{e//} = T_e$). However, the electron Lamor radius ρ_{ce} is assumed to be sufficiently small such that $k_\perp \rho_{ce} \ll 1$. Thus, while electron Landau damping will be treated in the present analysis, electron cyclotron damping shall be neglected. Collisional damping of the electron species is also neglected.

Using the notation of Stix [1], the dielectric tensor for the plasma may be written as

$$\mathbf{K} = \begin{bmatrix} S & -iD & 0 \\ iD & S & 0 \\ 0 & 0 & P \end{bmatrix} , \qquad (5)$$

where

$$S = 1 - \sum_s \frac{\omega_{ps}^2}{\omega^2 - \omega_{cs}^2} ,$$

$$D = \sum_s \frac{\omega_{ps}^2 \, \omega_{cs}}{\omega(\omega^2 - \omega_{cs}^2)} , \qquad (6)$$

$$P = 1 - \sum_i \frac{\omega_{pi}^2}{\omega^2} + 2\frac{\omega_{pe}^2}{\omega^2}\zeta_0^2\left[1 + \zeta_0 Z(\zeta_0)\right] \quad .$$

In the above expressions, ω_{cs} and ω_{ps} are respectively the cyclotron frequency and plasma frequency of species s. The plasma dispersion function is denoted by $Z(\zeta_0)$, its argument being

$$\zeta_0 = \frac{\omega - k_{//} V_{de}}{k_{//}\left(\frac{2 k_B T}{m_e}\right)^{1/2}} \quad ,$$

V_{de} being the drift velocity of the electron species.

The electron contributions to the above dielectric tensor are obtained by expanding the warm plasma dielectric tensor [9] to zero order in $k_\perp \rho_{ce}$. Using the large argument approximation for the plasma dispersion function, the electron contribution to S and D then reduces to the above cold plasma form.

The effect of ion collisional damping is included in the above dielectric tensor by introducing an effective complex mass m_i^* given by

$$m_i^* = m_i\left(1 + i\frac{\nu_i}{\omega}\right) .$$

thus rendering the ion cyclotron frequencies ω_{ci} complex [8], [10].

Substituting equation (5) into (1) using the expressions (2) then yields

$$k_{//}\frac{de_z^n}{dr} + \left(S - k_{//}^2\right)e_r^n - i\mathcal{D}e_\theta^n = 0 \quad , \tag{7}$$

$$\frac{d}{dr}\left(\frac{1}{r}\frac{d}{dr}\left(r e_\theta^n\right)\right) + \left(S - k_{//}^2\right)e_\theta^n + i\mathcal{D}e_r^n = 0 \quad , \tag{8}$$

$$k_{//}\frac{1}{r}\frac{d}{dr}(r\epsilon_r^n) - \frac{1}{r}\frac{d}{dr}\left(r\frac{d\epsilon_z^n}{dr}\right) - \mathcal{P}\epsilon_z^n = 0 \quad , \tag{9}$$

where $(\mathcal{S}, \mathcal{D}, \mathcal{P}) = \frac{\omega^2}{c^2}(S, D, P)$, and $k_{//} = \frac{n\pi}{L}$.

Considering solutions of equations (7) - (9) of the form

$$\begin{aligned} \epsilon_r^n &= \sum_j A_j^n J_1(k_{\perp j} r) \quad , \\ \epsilon_\theta^n &= \sum_j \varepsilon_{2j} A_j^n J_1(k_{\perp j} r) \quad , \\ \epsilon_z^n &= \sum_j \varepsilon_{3j} A_j^n J_0(k_{\perp j} r) \quad , \end{aligned} \tag{10}$$

yields the following dispersion relation

$$\begin{aligned} &(\mathcal{S} - k_{//}^2)(\mathcal{S} - k_{//}^2 - k_{\perp j}^2)(k_{\perp j}^2 - \mathcal{P}) \\ &\quad + k_{//}^2 k_{\perp j}^2 (\mathcal{S} - k_{//}^2 - k_{\perp j}^2) - \mathcal{D}^2 (k_{\perp j}^2 - \mathcal{P}) = 0 \quad . \end{aligned} \tag{11}$$

This quadratic equation in $k_{\perp j}^2$ therefore yields, for each value of $k_{//}$, two perpendicular wavenumbers given by

$$k_{\perp j}^2 = \frac{-b \pm (b^2 - 4ac)^{1/2}}{2a} \quad , \tag{12}$$

where $a = \mathcal{S}$, $b = (k_{//}^2 - \mathcal{S})(\mathcal{S} + \mathcal{P}) + \mathcal{D}^2$, $c = \mathcal{P}[(k_{//}^2 - \mathcal{S})^2 - \mathcal{D}^2]$.

Substituting expression (2) into equation (8) and (9) also gives

$$\varepsilon_{2j} = \frac{i\mathcal{D}}{k_{//}^2 + k_{\perp j}^2 - \mathcal{S}} \quad , \qquad \varepsilon_{3j} = \frac{-k_{//}\, k_{\perp j}}{k_{\perp j}^2 - \mathcal{P}} \quad . \tag{13}$$

(i) In the vacuum region k (k = II - IV) :

The fields in each of the vacuum regions are obtained by setting K = I in equation (1), thus, $\mathcal{S} = \mathcal{P} = \omega^2 / c^2$ and $\mathcal{D} = 0$. We consider solutions for the Fourier amplitudes of the electric wavefields of the form

$$\begin{aligned} e_r^n &= C_k^n I_1(k_0 r) + D_k^n K_1(k_0 r) \quad , \\ e_\theta^n &= F_k^n I_1(k_0 r) + G_k^n K_1(k_0 r) \quad , \\ e_\theta^n &= \frac{k_0}{k_{//}} \left\{ C_k^n I_0(k_0 r) + D_k^n K_0(k_0 r) \right\} \quad , \end{aligned} \tag{14}$$

which satisfy the vacuum condition $\nabla \cdot \mathbf{E} = 0$. The vacuum wavenumber is given by

$$k_0^2 = k_{//}^2 - \frac{\omega^2}{c^2} \quad .$$

The 14 coefficients of the wavefield amplitudes,

$$A_1^n, \; A_2^n, \; C_k^n, \; D_k^n, \; F_k^n \text{ and } G_k^n, \qquad k = II, III, IV$$

are determined by the boundary conditions at the four surfaces, r = p, u, s, q. At the plasma-vacuum interface, it is assumed that there are no surface currents or charges, consistent with the inclusion of electron inertia in the plasma model. The Faraday shield is assumed to eliminate completely any axial electric field which may be coupled to the plasma from the antenna, while not affecting the azimuthal electric field. The antenna is treated as a current sheet flowing in the azimuthal direction only and having no azimuthal

dependence. The imposed current per unit length J^+, can be expressed in terms of the following Fourier series:

$$J^+(z) = \sum_{n=1}^{\infty} j_n^+ \sin \frac{n\pi}{L} z \quad . \tag{15}$$

The cylindrical shell at $r = q$ is assumed to be perfectly conducting in both the azimuthal and axial directions.

With the above considerations, the appropriate boundary conditions can then be written as follows:

At $r = p$: E_θ, E_z, B_θ and B_z are continuous,

$r = u$: E_θ, E_z and B_z are continuous, and $E_z = 0$,

$r = s$: E_θ, E_z and B_θ are continuous, and $[B_z]_{r=s} = \mu_0 J^+$,

$r = q$: $E_\theta = E_z = 0$.

Substituting the expressions for the wavefields into the above boundary conditions yields a set of fourteen equations for the required coefficients of the wavefield amplitudes.

Both collisional and collisionless damping processes in the plasma result in power being coupled from the antenna to the plasma. The complex power input to the plasma-antenna system, averaged over a period of oscillation, is given by

$$P = \frac{1}{2} \int_V \mathbf{J}^+ \cdot \mathbf{E} \; dV \quad , \tag{16}$$

where the integral is taken over the volume of the antenna. For an antenna consisting of a coil wound with $\nu(z)$ turns per unit length, $J^+(z) = I_0\,\nu(z)$, where I_0 is the antenna current amplitude. If the plasma loading of the antenna is modelled by a complex impedance in series with the impedance of the antenna, we may write the power input as

$$P = \frac{1}{2} I_0^2 \left\{ R_c + R_p - i\omega(L_c + L_p) \right\} .$$

The resistive and reactive components of the power input to the plasma are then, respectively,

$$P_R = \frac{1}{2} I_0^2 R_p \quad , \qquad P_I = \frac{1}{2} I_0^2 \omega L_p \quad . \tag{17}$$

Substituting equations (2) and (15) into equation (16) then yields for the power input to the plasma

$$P = P_R + P_I = \sum_{n=1}^{\infty} P_n = \sum_{n=1}^{\infty} \left\{ \frac{\pi s L_c}{2} j_n^+ e_\theta^n(s) \right\} \quad . \tag{18}$$

3. Numerical examples

Using the theory outlined in Section 2, calculations have been undertaken to determine the wavefields and power coupled to the plasma associated with the excitation of ion cyclotron modes. Here, we shall present results for cases of relevance to an experimental investigation reported in the companion paper [2]. A neon plasma is considered, comprised of two ion species Ne^{20} and Ne^{22} in approximately their natural relative abundance ($\beta_1 = 0.9$ and $\beta_2 = 0.1$, respectively, where $\beta_j = n_j / n_e$). The parameters used to obtain the results presented here are, unless otherwise specified, as given in Table 1.

The antenna structure considered in the present study was chosen to preferentially excite the fourth axial mode of the plasma cavity (n = 4). Corresponding to the experimental realization [2], we consider an antenna comprised of four separate modules having a current distribution given by

$$J^{+}(z) = \begin{cases} I_0 \nu_0 & \text{for} \quad -\frac{3b}{2} - \frac{a}{2} \le z \le -\frac{3b}{2} + \frac{a}{2} \\ & \quad \frac{b}{2} - \frac{a}{2} \le z \le \frac{b}{2} + \frac{a}{2} \\ -I_0 \nu_0 & \text{for} \quad -\frac{b}{2} - \frac{a}{2} \le z \le -\frac{b}{2} + \frac{a}{2} \\ & \quad \frac{3b}{2} - \frac{a}{2} \le z \le \frac{3b}{2} + \frac{a}{2} \\ 0 & \text{otherwise} \end{cases} \tag{19}$$

The width and separation of the modules are chosen to be, respectively, $a = \lambda / 4$ and $b = \lambda / 2$, where the periodicity length of the antenna structure is given by $\lambda = L / 2$. Due to the chosen symmetry of this antenna, contributions to the antenna current exist only from every eighth axial mode. (The Fourier components of the antenna current are shown in figure 4(a).) A value of $I_0 \nu_0 = 18.5$ A cm^{-1} was considered, corresponding to a current of 50 A passing through antenna modules with 25 turns [2].

3.1 Perpendicular wavenumber

Before examining the power deposited in the plasma due to the excitation of the ion cyclotron modes, it is of interest to investigate the influence of various physical processes on the wavenumber of the modes. For a fixed parallel wavenumber $k_{//}$, the dispersion relation (11) can be solved to yield for the ion cyclotron wave branch

$$k_{\perp 1}^2 = \frac{\mathcal{P}}{S}\left(S - k_{//}^2\right) \quad , \qquad k_{\perp 2}^2 \approx S - k_{//}^2 \quad , \tag{20}$$

under the condition that

$$k_{\perp j}^2 \gg \frac{\mathcal{D}^2}{S} \; ; \; \mathcal{D}\left|\frac{\mathcal{P}}{S}\right|^{1/2} \quad . \tag{21}$$

Since $|\mathcal{P}| \gg S$ for the cases of interest in the present study, $|k_{\perp 1}| \gg |k_{\perp 2}|$. Therefore, under the above conditions, $k_{\perp 1}$ plays a dominant role in determining the radial structure of the wavefields [8].

It can be observed that the condition (21) is clearly not satisfied for $S \approx 0$. For a plasma comprised of two ion species, this occurs when the wave frequency is in the close vicinity of the ion-ion hybrid frequency given by

$$\omega_h^2 = \omega_{c1}\,\omega_{c1}\,\frac{\beta_1\,\omega_{c2} + \beta_2\,\omega_{c1}}{\beta_1\,\omega_{c1} + \beta_2\,\omega_{c2}} \quad . \tag{22}$$

Calculations have been undertaken of the perpendicular wavenumbers associated with the fourth axial mode of the plasma cavity (for which, $k_{//} = 2.33\ m^{-1}$). In figure 2 is shown, for four values of electron temperature, the dependence of the real and imaginary parts of $k_{\perp 1}$ on frequency for $\omega \approx \omega_{ci}$. This figure shows that for the range of conditions considered, electron kinetic effects play a dominant role in determining $k_{\perp 1}$, even for very low electron temperatures. It can also be noted that in the vicinity of the frequency $f \approx f_h = 211.4$ kHz, the wave modes suffer strong damping, as indicated by the large negative value of the imaginary part of $k_{\perp 1}$.

Since $k_{\perp 1}$ is the dominant perpendicular wavenumber, it can be shown that modes are excited in the plasma cavity if

$$k_{\perp 1} p \approx a_\ell \quad , \tag{23}$$

where a_ℓ is the ℓ^{th} zero of the J_1 Bessel function. The subscript ℓ thus denotes the radial mode number. Note that, from equation (20), $k_{\perp 1}$ is dependent on $\mathcal{P}$ and hence on electron kinetic effects, whereas $k_{\perp 2}$ is independent of $\mathcal{P}$.

3.2 Power input to plasma

The power transferred from the antenna to the plasma has been calculated, using equation (18), for the same set of parameters as above. The frequency dependence of the power input into the first 100 axial modes is shown in figure 3. These results show that if electron kinetic effects are neglected, several narrow resonances are observed for the small value of collision frequency considered ($\nu_i/\omega \approx 0.02$). These resonances can be identified as associated with different axial and radial modes, each satisfying equation (23). The two principle ($n = 4$, $\ell = 1$) modes are located just below each of the ion cyclotron frequencies.

Figure 3 shows that electron Landau damping associated with even low electron temperatures substantially modifies the power input to the plasma. The frequency dependence of the power loading now exhibits a broad maximum, which is split into two peaks due to the strong damping that occurs for $\omega \approx \omega_h$. The peak power input to the plasma is considerably reduced compared to that calculated neglecting electron kinetic effects. Note that the lowest frequency peak appears at a frequency in the close vicinity of ω_{c2}, and is therefore presumably severely influenced by the presence of ion cyclotron damping. In practice, the separation of the resonance maximum into two peaks may therefore not be observable.

The maximum of the power loading observed in the presence of finite electron temperature appears at a frequency $\omega > \omega_{c1}$. The position of the maximum is strongly influenced by electron temperature, shifting to higher frequency as the electron temperature increases. Except for very low electron temperatures, the maximum loading occurs at a frequency sufficiently remote from the ion cyclotron frequencies to be unaffected by ion cyclotron damping.

In figure 4(a) is presented both the Fourier amplitudes of the first 100 axial modes of the antenna current. Figure 4(b) shows the power deposited into the various axial modes assuming electron kinetic effects are negligible. The excitation frequency was chosen to correspond to that which yields the maximum power input to the n = 4 mode (i.e., f = 219.8 kHz). It is seen that essentially all the power ($\approx$ 98 %) is deposited into the n = 4 mode. The corresponding mode decomposition for a plasma with T_e = 5 eV, for f = 253.4 kHz, is presented in figure 4(c). Due to the stronger damping of the principal axial mode, only $\approx$ 76 % of the total power is deposited into this mode. Thus, the contribution of the higher order axial modes plays an important role in determining the wavefields in the plasma.

3.3 Wavefields

The radial and axial dependence of the three electric wavefield components, for the same parameters as used for figure 4, are shown in figure 5. For both of the cases shown in this figure, the E_θ component is essentially the vacuum field of the antenna; there is negligible modification due to the presence of the plasma. For the case T_e = 0, figure 5(a) shows that the E_r and E_z components, which are zero in the absence of the plasma, exhibit a structure similar to the (n = 4, ℓ = 1) eigenmode. This is consistent with the above observation that, for the frequency considered, this mode is selectively excited in

the plasma. For $T_e = 5$ eV, the axial mode selectivity of the antenna is much poorer. This is most marked in the axial dependence of the E_z wavefield, which is strongly peaked at the end of each antenna module. Due to the strong Landau damping associated with finite electron temperature, the axial electric field does not propagate a significant distance away from the antenna module.

For the parameters of the present investigation, the perpendicular wavenumber is much greater than the parallel wavenumber, thus $\mathbf{k} \approx k_\perp \mathbf{r}$. Figure 5 shows that the electric wavefield vector is also essentially oriented in the radial direction. Thus, $\mathbf{k}$ is approximately parallel to $\mathbf{E}$, and hence the ion cyclotron modes considered in the present study have a strong electrostatic character.

In a manner similar to the E_θ wavefield, the radial and axial components of the magnetic wavefield are calculated to be essentially the vacuum field. Figure 6 shows that for the parameters considered, the B_θ wavefield resembles the Bessel function $J_1(k_{\perp 1} r)$, where $k_{\perp 1}$ corresponds to the lowest radial mode given by equation (23); its shape appears to be insensitive to the effects of finite electron temperature.

Figures 5 and 6 shows that the presence of electron Landau damping results in a substantial decrease in the amplitude of the field components associated with wave excitation. A more detailed examination of its influence on the field amplitudes is presented in figure 7. This figure shows, for four values of electron temperature, the frequency dependence of the amplitude and phase of the B_θ component calculated at the mid-radius of the plasma, midway between two antenna modules.

3.4 Effect of electron drift

The theory developed in Section 2 treats cavity modes that can be considered as combinations of positive and negative propagating waves. For the case of no electron drift ($V_{de} = 0$), the amplitude of the axial wave number is the same in both directions. However, the introduction of electron drift results in an asymmetry due to the inclusion of the electron kinetic effects. Thus the present formalism can not be applied in a straightforward fashion. Nevertheless, it can be shown that the effect of electron drift can be approximated by averaging the difference between the results calculated for cavity modes with $V_{de} > 0$ and $V_{de} < 0$, under the condition that the amplitude of the cavity wavefields for these two modes is approximately equal.

Introducing a finite value of V_{de} into the calculations yields two effects, the resonant frequency of the cavity modes are shifted, and the wavefield amplitudes modified. In figure 8 is plotted the frequency at which maximum power loading of the n = 4 mode occurs, as a function of drift velocity, for the parameters considered in Table 1. It can be observed for $V_{de} < 0$ there is a shift in the resonant frequency to lower values. For $V_{de} > 0$, a shift of approximately equal magnitude towards higher frequencies is calculated. It is also calculated that over the range of drift velocities considered in figure 8, the maximum power input to the plasma is essentially unchanged. (This is a consequence of the fact that, for the parameters considered, the resonant frequency $\omega_r >> |k_{//} V_{de}|$.) Therefore, the average of the $V_{de} > 0$ and $V_{de} < 0$ calculations is approximately the same as the $V_{de} = 0$ result. It is thus concluded that, for the parameters considered, the effect of electron drift on the resonant frequency is not significant.

4. Conclusions

Ion cyclotron modes excited in a low density, cylindrical plasma cavity have been described. For the conditions considered, it has been shown that these modes have a long parallel wavelength, and are essentially electrostatic in nature. It has been shown that these modes are strongly influenced by electron dynamics. Even for low electron temperatures, the dominant dissipative mechanism was found to be electron Landau damping. Strong peaks in the power loading as a function of frequency have been calculated if electron kinetic effects are neglected. However, in the presence of electron Landau damping, the power loading has been shown to exhibit only a broad resonance in the vicinity of the ion cyclotron frequencies, even for low electron temperatures.

Acknowledgements

Discussions with P.J. Paris and M.Q. Tran are gratefully acknowledged. This work was partially supported by the Fonds National Suisse de la Recherche Scientifique.

References

[1] T.H. Stix, *Theory of Plasma Waves*, McGraw-Hill, New York (1962).

[2] M.L. Sawley and P.J. Paris, companion paper.

[3] J.C. Hosea and R.M. Sinclair, *Physical Review Letters*, **23**, 3 (1969).

[4] J.C. Hosea and R.M. Sinclair, *The Physics of Fluids*, **13**, 701 (1970).

[5] S. Yoshikawa, M.A. Rothman and R.M. Sinclair, *Physical Review Letters*, **14**, 214 (1965).

[6] C.R. Skipping, M.E. Oakes and H. Schlüter, *The Physics of Fluids*, **12**, 1886 (1969).

[7] H. Schlüter and G. Shürger, *Z. Naturforsch. A*, **30**,1600 (1975).

[8] M.L. Sawley and M.Q. Tran, Lausanne Report LRP 206/82 (1982).

[9] K. Miyamoto, *Plasma Physics for Nuclear Fusion*, MIT Press, Cambridge (1980).

[10] G. Muller, *Plasma Physics*, **16**, 813 (1974).

electron density	$n_e = 10^{11}$ cm^{-3}
axial magnetic field	$B_0 = 3$ kG
electron drift velocity	$V_{de} = 0$
ion cyclotron frequencies	$\omega_{c1} = 230.4$ kHz $\omega_{c2} = 209.4$ kHz
effective collision frequency	$\nu_i = 5$ kHz
plasma length	L = 540 cm
plasma radius	p = 2.5 cm
Faraday shield radius	u = 5 cm
antenna radius	s = 6 cm
conducting shell radius	q = 20 cm

Table 1. Plasma and antenna parameters used in the calculations

Figure Captions

Figure 1. Schematic diagram of the partially plasma filled cavity.

Figure 2. Frequency dependence of (a) the real part, and (b) the imaginary part of the perpendicular wavenumber $k_{\perp 1}$ of the n = 4 mode and the four values of electron temperature indicated.

Figure 3. Frequency dependence of (a) the real part, and (b) the imaginary part of the power input into the plasma for the four values of electron temperature indicated.

Figure 4. Fourier amplitudes of the first 100 axial modes of (a) the antenna current, and the power deposited into the plasma for (b) $T_e = 0$, and (c) $T_e = 5$ eV.

Figure 5. Radial and axial dependence of the three components of the electric wavefield, for (a) $T_e = 0$, and (b) $T_e = 5$ eV.

Figure 6. Radial and axial dependence of the in-phase component of the azimuthal component of the magnetic wavefield, for (a) $T_e = 0$, and (b) $T_e = 5$ eV.

Figure 7. Frequency dependence of (a) the in-phase component, and (b) the out-of-phase component of the azimuthal magnetic wavefield B_θ, calculated at the mid-radius of the plasma midway between two antenna modules, for the four values of electron temperature indicated.

Figure 8. Dependence of the resonant frequency of the n = 4 mode on the bulk electron drift velocity.

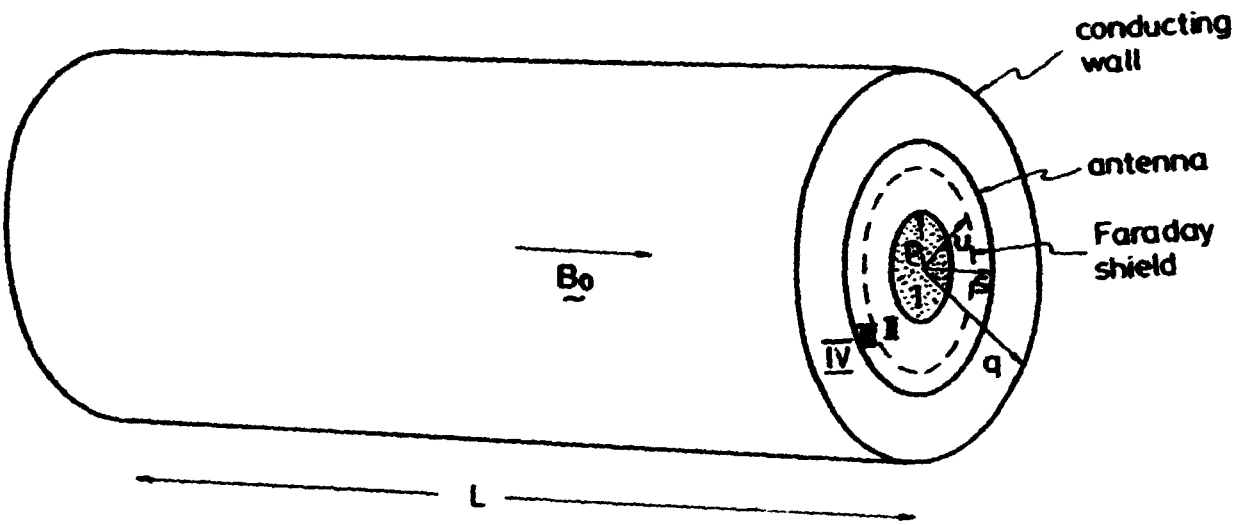

Figure 1

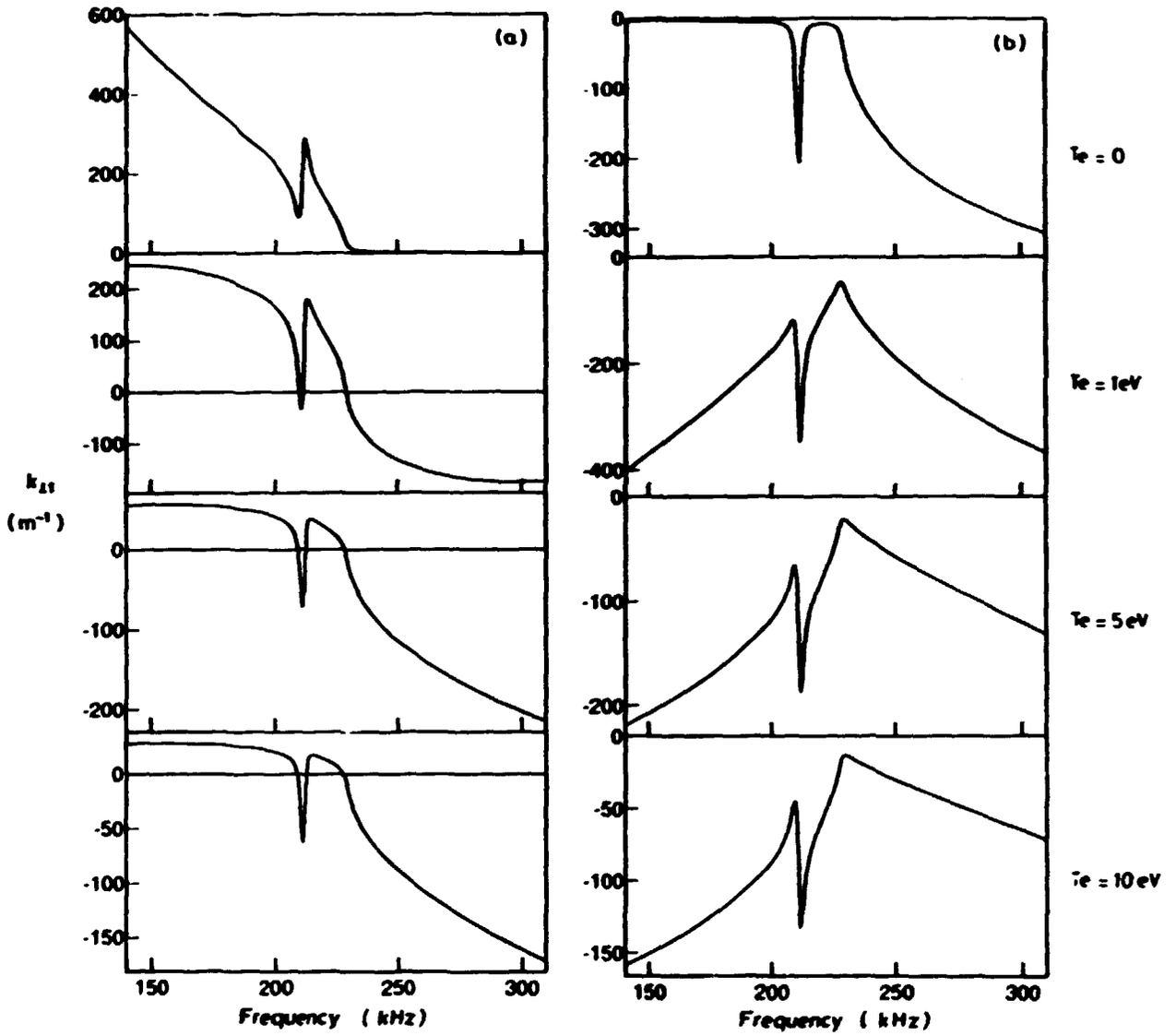
(a)
(b)
600
400
200
0
200
100
0
-100
0
-100
-200
0
-50
-100
-150
0
-100
-200
0
-200
-400
0
-100
-200
0
-50
-100
-150
k_{zi}
(m^{-1})
Te = 0
Te = 1eV
Te = 5eV
Te = 10eV
150
200
250
300
Frequency (kHz)
Frequency (kHz)

Figure 2

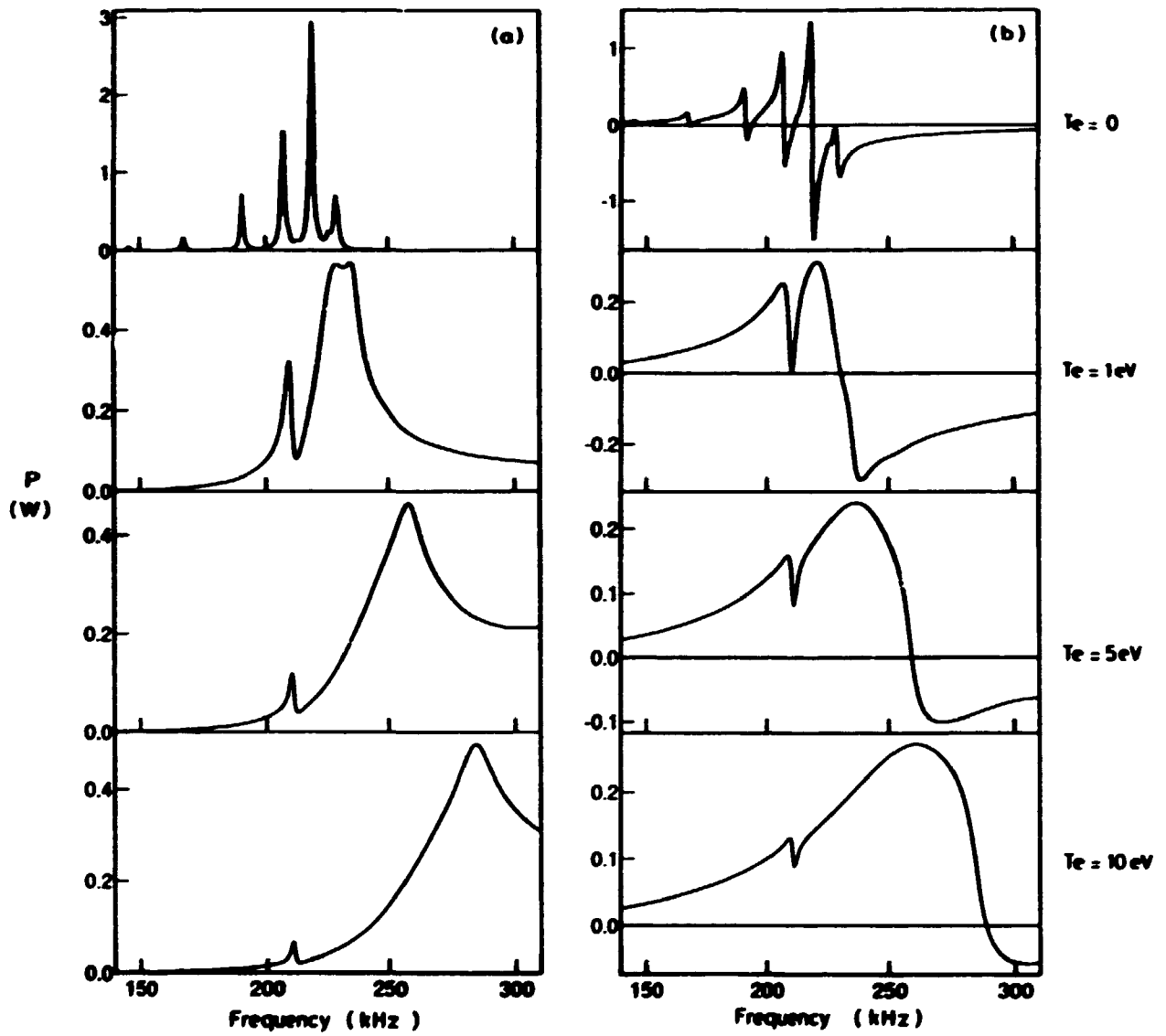
(a)
(b)
P
(W)
Te = 0
Te = 1eV
Te = 5eV
Te = 10eV
Frequency (kHz)
Frequency (kHz)
150
200
250
300

Figure 3

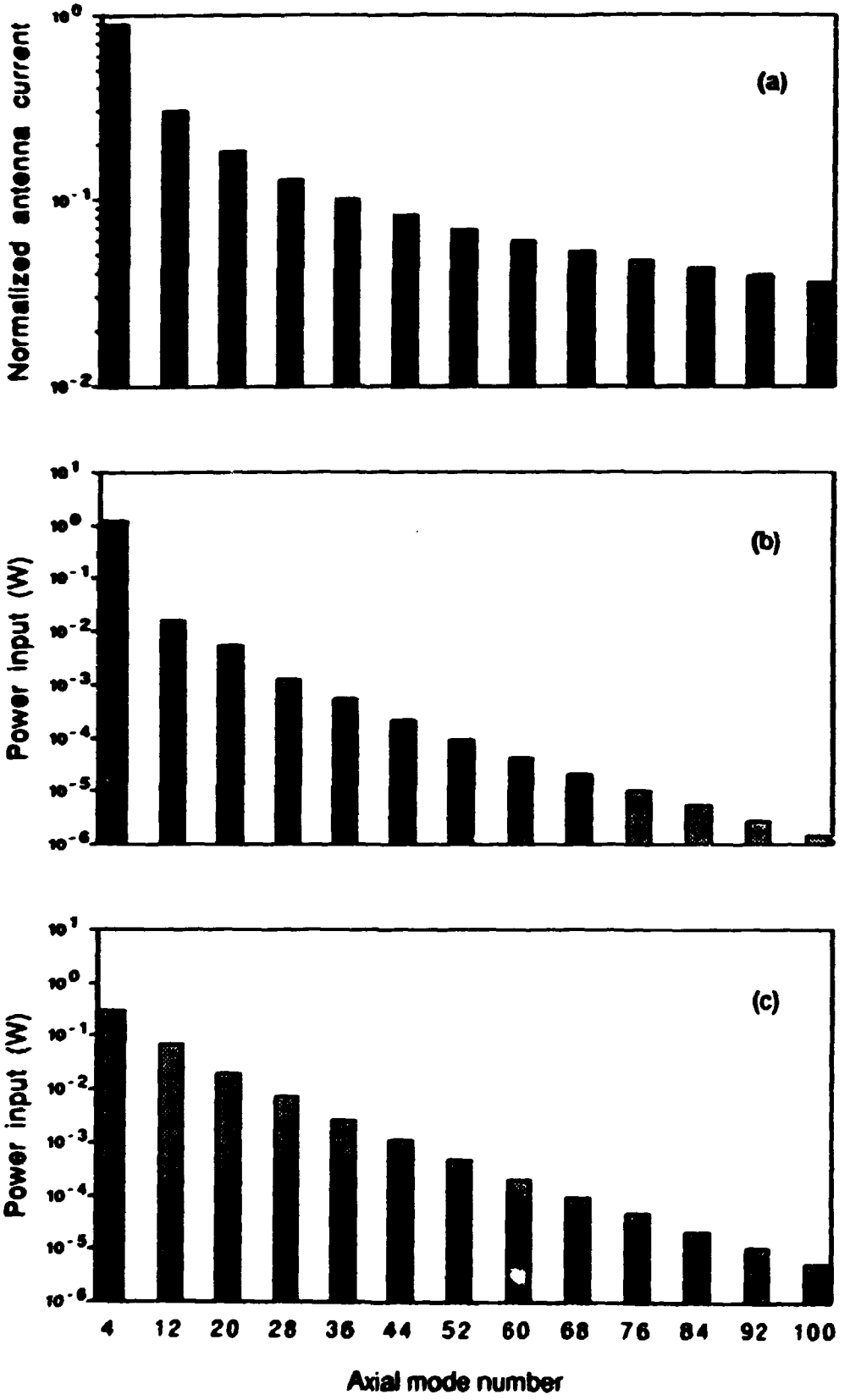
Normalized antenna current
(a)
Power input (W)
(b)
Power input (W)
(c)
4
12
20
28
36
44
52
60
68
76
84
92
100
Axial mode number

Figure 4

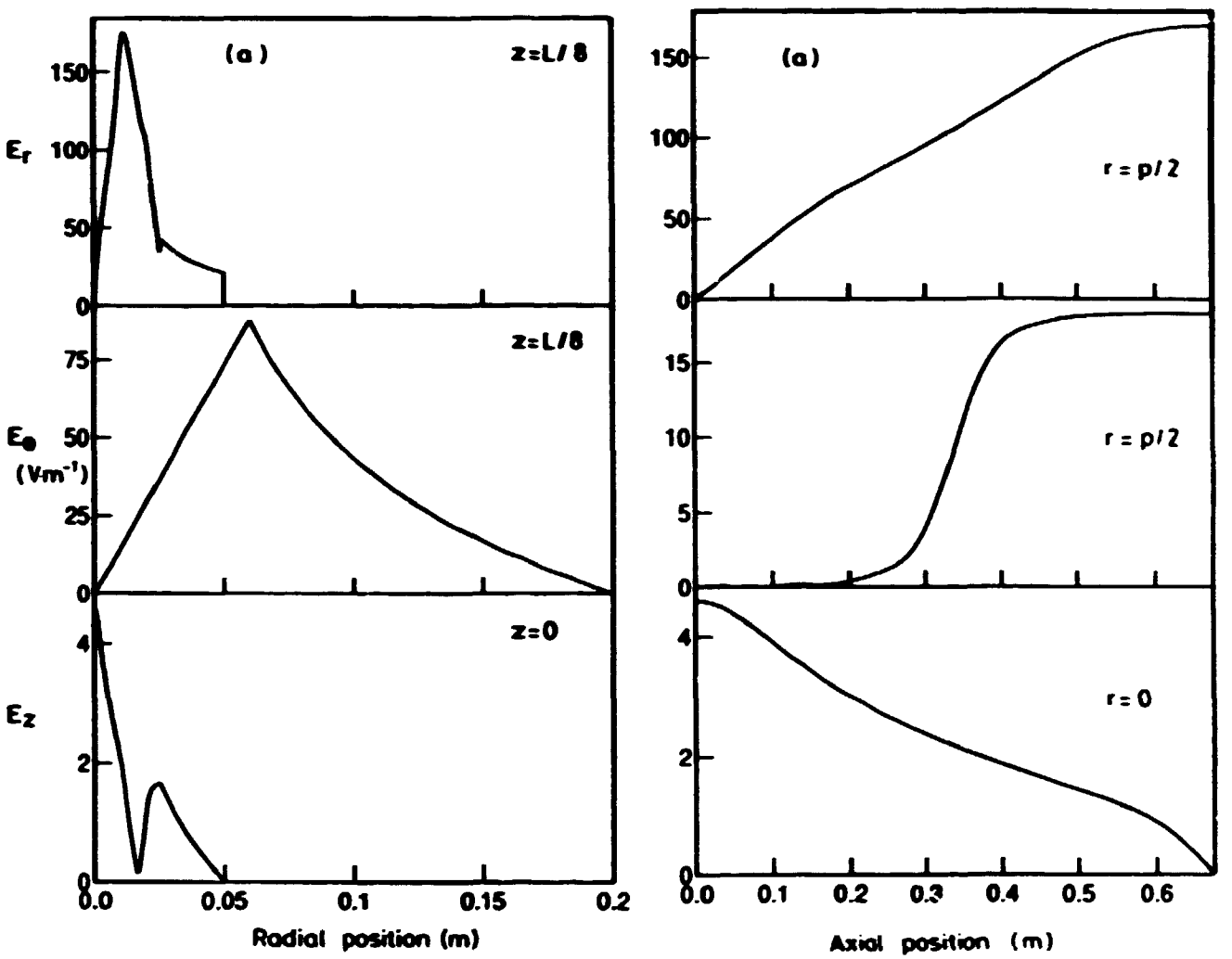
(a)
z=L/8
E_r
150
100
50
0
z=L/8
E_θ
(Vm^{-1})
75
50
25
0
z=0
E_z
4
2
0
0.0
0.05
0.1
0.15
0.2
Radial position (m)
(a)
150
100
50
0
r = p/2
15
10
5
0
r = p/2
4
2
0
r = 0
0.0
0.1
0.2
0.3
0.4
0.5
0.6
Axial position (m)

Figure 5(a)

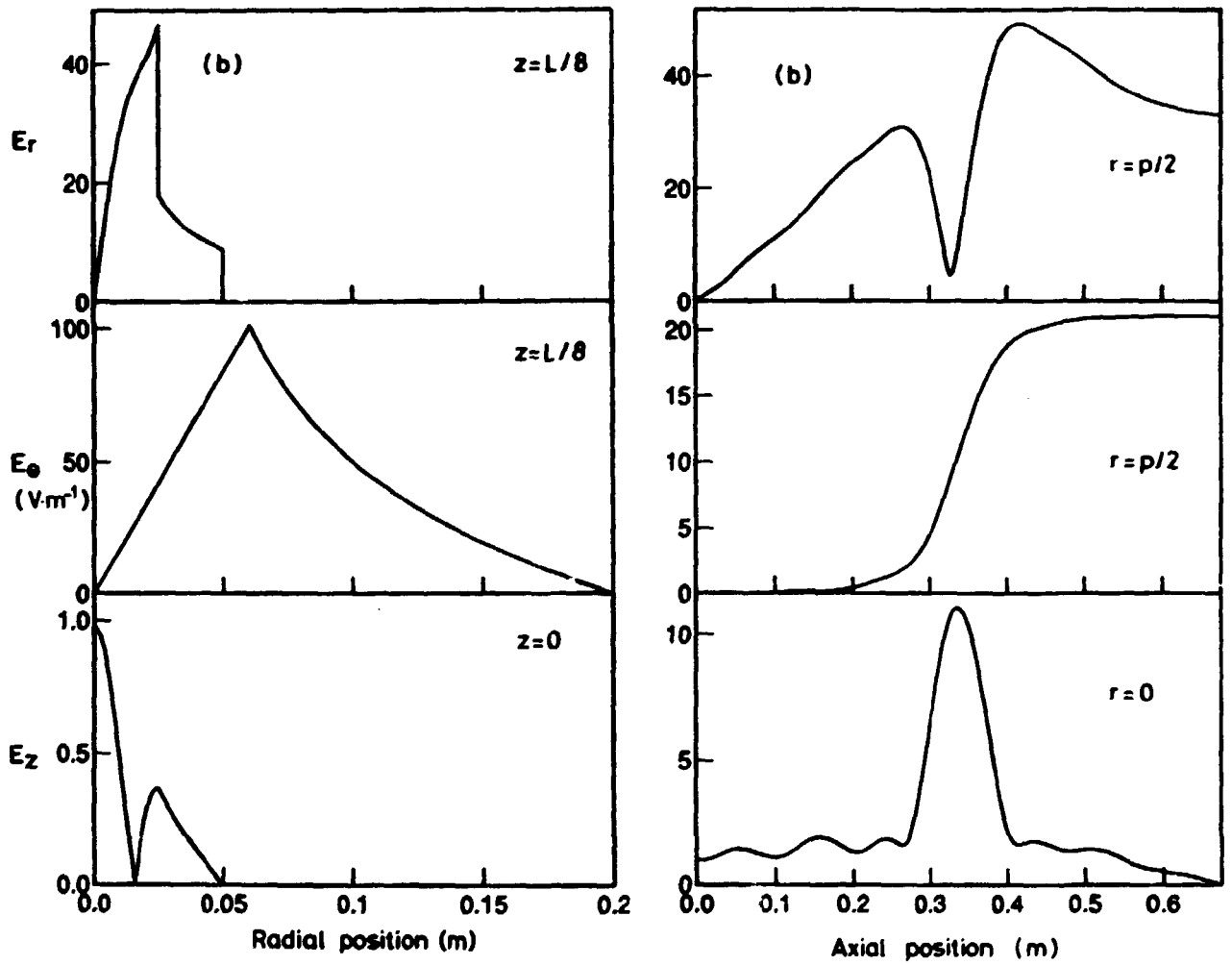
(b)
z=L/8
E_r
40
20
0
z=L/8
E_θ (V·m^{-1})
100
50
0
z=0
E_z
1.0
0.5
0.0
0.0
0.05
0.1
0.15
0.2
Radial position (m)
(b)
r=p/2
40
20
0
r=p/2
20
15
10
5
0
r=0
10
5
0
0.0
0.1
0.2
0.3
0.4
0.5
0.6
Axial position (m)

Figure 5(b)

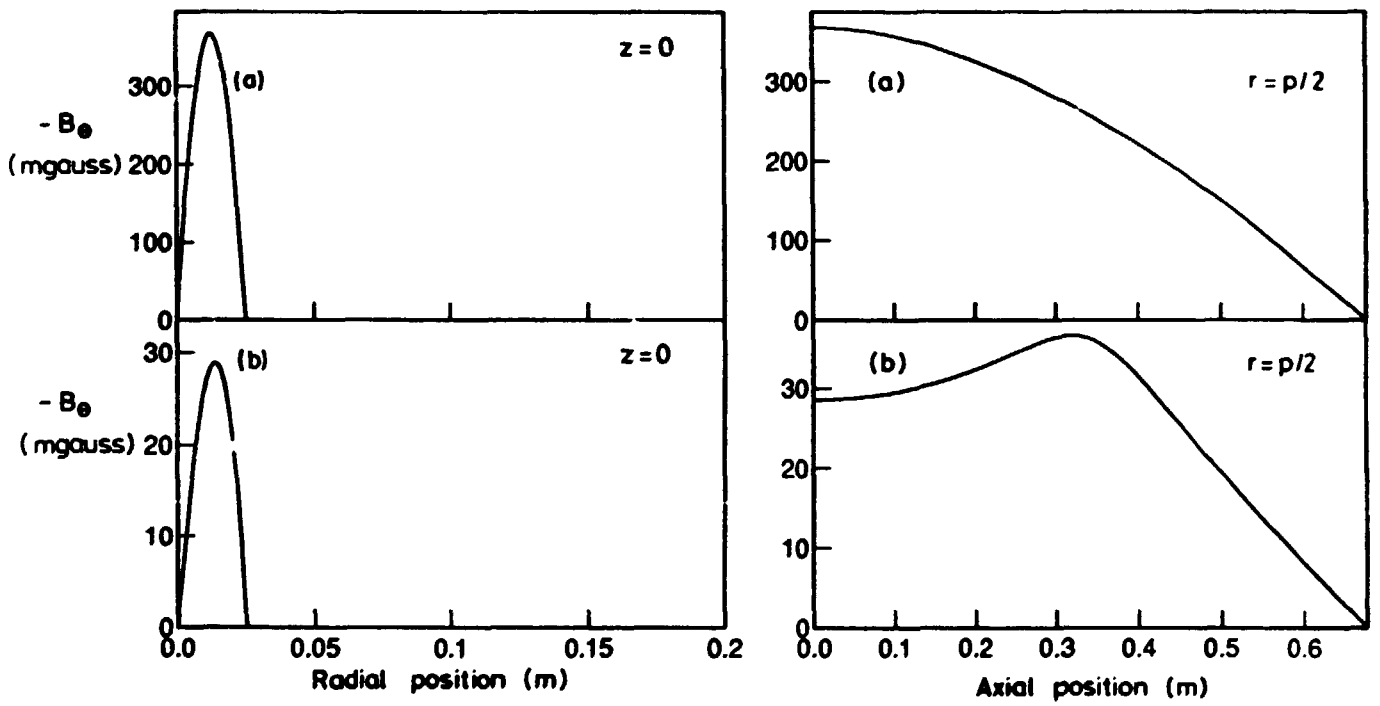
z = 0
(a)
300
200
100
0
- Bθ
(mgauss)
(b)
z = 0
30
20
10
0
0.0
0.05
0.1
0.15
0.2
Radial position (m)
(a)
r = p/2
(b)
r = p/2
0.0
0.1
0.2
0.3
0.4
0.5
0.6
Axial position (m)

Figure 6

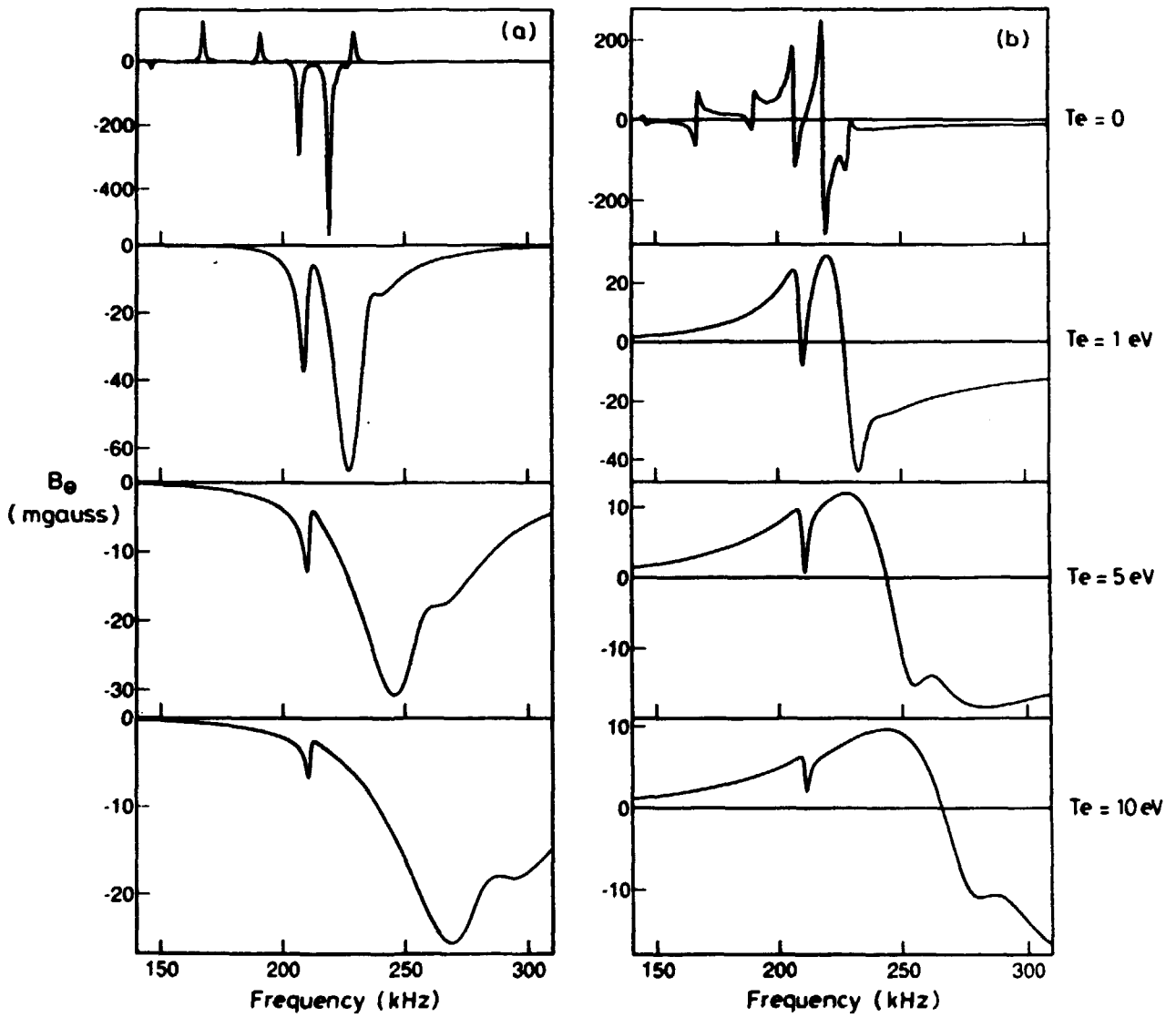
(a)
(b)
Te = 0
Te = 1 eV
Te = 5 eV
Te = 10 eV
B_θ
(mgauss)
Frequency (kHz)
Frequency (kHz)

Figure 7

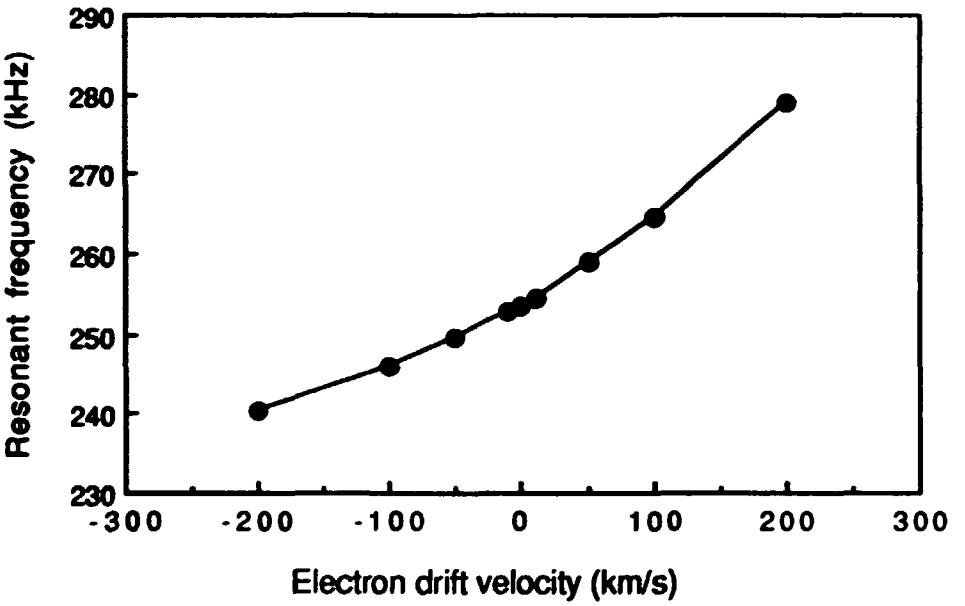
290
280
270
260
250
240
230
Resonant frequency (kHz)
-300
-200
-100
0
100
200
300
Electron drift velocity (km/s)

Figure 8